AAS 08-111

A GENERAL BANG-BANG CONTROL METHOD FOR LORENTZ AUGMENTED ORBITS

Brett Streetman* **and Mason A. Peck** †

This paper presents a general control method for Lorentz Augmented Orbits (LAOs). A spacecraft carrying an electrostatic charge moves through the geomagnetic field. The resulting Lorentz force is used to evolve the spacecraft's orbit. Concepts relating to LAO system design are explored. A high degree and order spherical harmonic expansion is used to model the magnetosphere. The space of longitude and latitude is partitioned in a physically meaningful way. Within any given partition, certain orbital elements tend to evolve in a certain directions under a constant spacecraft charge. A bang-bang controller is implemented with switching only at partition boundaries. Control sequences are developed to produce maneuvers such as a LEO plane change from an inclined to an equatorial orbit.

INTRODUCTION

Propellantless propulsion opens new possibilities for spacecraft missions. One form of propellantless propulsion is the Lorentz Augmented Orbit (LAO). The idea of LAO was first presented by Peck,[1] and further examined through our later work.[2,3] A body with net charge q moving in a magnetic field $\mathbf{B}$ is affected by a Lorentz force

$$\mathbf{F}_L = q(\mathbf{v} - \omega_E \hat{\mathbf{n}} \times \mathbf{r}) \times \mathbf{B} \tag{1}$$

where $\mathbf{r}$ is the position of the spacecraft in an Earth-centered, inertial reference frame, $\mathbf{v}$ is the spacecraft velocity in this frame, ω_E is the spin rate of the Earth, and $\hat{\mathbf{n}}$ is a unit vector along the spin axis of the Earth. The velocity correction $(-\omega_E \hat{\mathbf{n}} \times \mathbf{r})$ is required because the magnetic field $\mathbf{B}$ is constant in an Earth-fixed frame. The charge-to-mass ratio, $\frac{q}{m}$, of spacecraft determines the magnitude of the acceleration applied by the Lorentz force. The direction of this acceleration is fixed by the velocity of the spacecraft and the magnetic field at its location. Because the charge on the spacecraft can be maintained solely with electrical power and because the Lorentz force acts externally, LAO technology represents propellantless propulsion. If $\frac{q}{m}$ is varied as a control input, an LAO can achieve novel orbits and applications.

Orbit perturbations on charged particles due to the Lorentz force have been observed in natural systems. Schaffer and Burns[4,5] and Hamilton[6] have studied these effects and derived various perturbation equations. They have shown that the Lorentz force acting on micron-sized, naturally charged dust grains creates significant changes in their orbits. This effect explains features seen in the ethereal rings of Jupiter. The dynamics of these charged dust grains is well understood in the context of naturally occurring systems. We wish to expand the available orbits and add controlled charging to exploit the Lorentz force for engineering applications through LAOs.

*Graduate Research Assistant, Department of Mechanical and Aerospace Engineering, Cornell University, 245 Upson Hall.

†Assistant Professor, Department of Mechanical and Aerospace Engineering, Cornell University, 212 Upson Hall.

Alternative propellantless propulsion systems that take advantage of the Lorentz force and spacecraft charging have been proposed. Electrodynamic tethers force current through a long conductor.[7] The current in this tether moving with the satellite creates a Lorentz force. By using a current in a wire rather than a space charge on the spacecraft, a tether can produce forces in directions an LAO spacecraft cannot. However, the direction of the tether must be controlled, while LAO is attitude independent. In addition to LAO, a charged spacecraft architecture has been proposed for formation flight.[8,9] The Coulomb Spacecraft Formation system makes use of the Coulomb force acting between two charged satellites, rather than the Lorentz force. While LAO is an absolute force, the Coulomb formation can produce only relative forces between nearby bodies.

Our earlier studies[1,2,3] present the dynamics of LAOs under simplified conditions, including greatly simplified magnetic field models. This study expands this analysis to include spherical-harmonic magnetic fields of arbitrary complexity. Overviews of the effect of the Lorentz force on an orbit and the general properties of the geomagnetic field are followed by new material on possible LAO system architectures. A discussion of the maneuver limitations introduced by the Lorentz force is presented, along with two possible LAO maneuvers.

Lorentz Perturbations

The effects of the Lorentz force on an orbit are studied using perturbation methods. We have previously shown that the change in orbital energy, E, of a charged spacecraft affected by an arbitrary magnetic field, $\mathbf{B}$, is given by[2]

$$\dot{E} = \frac{q}{m}\omega_E \left[(\mathbf{v}\cdot\hat{\mathbf{n}})(\mathbf{B}\cdot\mathbf{r}) - (\mathbf{v}\cdot\mathbf{r})(\hat{\mathbf{n}}\cdot\mathbf{B})\right] \tag{2}$$

To describe this position and velocity, we use an Earth-centered, inertial reference frame with spherical coordinates: radius r, colatitude ϕ, and azimuth angle θ, as displayed in Fig. 1. In these

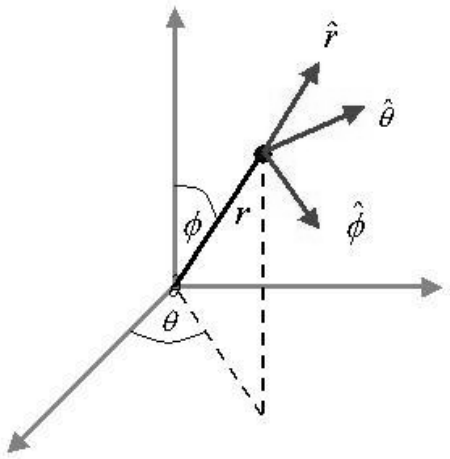

Figure 1 Spherical coordinates and unit vectors used.

coordinates, Eq. 2 can be expressed as

$$\dot{E} = \frac{q}{m}\omega_E \left[(r\mathbf{v}\cdot\hat{\mathbf{n}} - \cos\phi\mathbf{r}\cdot\mathbf{v})(\mathbf{B}\cdot\hat{\mathbf{r}}) + \sin\phi(\mathbf{r}\cdot\mathbf{v})(\mathbf{B}\cdot\hat{\phi})\right] \tag{3}$$

where $\hat{\mathbf{r}}$ and $\hat{\phi}$ are unit vectors in the r- and ϕ-directions, respectively. These unit vector are also depicted in Fig. 1.

Change in vector angular momentum is also found from perturbation methods:[2]

$$\dot{\mathbf{h}} = \frac{q}{m}(\mathbf{B}\cdot\mathbf{r})\mathbf{v} - \frac{q}{m}(\mathbf{r}\cdot\mathbf{v})\mathbf{B} - \frac{q}{m}\omega_E(\mathbf{B}\cdot\mathbf{r})(\hat{\mathbf{n}}\times\mathbf{r}) \tag{4}$$

The information contained in Eqs. 2 and 4 is used to obtain the derivatives of other orbital elements. Equation 4 leads to an expression for the derivative of inclination, i, is[10]

$$\frac{di}{dt} = \frac{\dot{h}\cos i - \dot{\mathbf{h}}\cdot\hat{\mathbf{n}}}{h\sin i} \tag{5}$$

where h is the scalar orbital angular momentum. In the spherical coordinates, Eq. 5 becomes

$$\begin{aligned}\frac{di}{dt} &= \frac{-1}{h\omega_E\sin i}\dot{E} + \frac{q}{m}\frac{\cos i}{h^2\sin i}\Big[\omega_E r^2\left(r\mathbf{v}\cdot\hat{\mathbf{n}} - \cos\phi\mathbf{r}\cdot\mathbf{v}\right)(\mathbf{B}\cdot\hat{\mathbf{r}}) \\ &\quad + \frac{h\cos i}{\sin\phi}(\mathbf{r}\cdot\mathbf{v})(\mathbf{B}\cdot\hat{\phi}) + h\sin i\cos(\theta-\Omega)(\mathbf{r}\cdot\mathbf{v})(\mathbf{B}\cdot\hat{\theta})\Big]\end{aligned} \tag{6}$$

where Ω is the right ascension of the orbit. The first term in Eq. 6 shows that changes in inclination are closely related to changes in orbital energy, especially for orbits that are near circular or polar. This term generally dominates this equation. An expression for the change in eccentricity, e, is[10]

$$\dot{e} = \left[\frac{a}{\mu}(1-e^2)\right]^{1/2}\left\{(\mathbf{F_L}\cdot\hat{\mathbf{r}})\sin\nu + [\mathbf{F_L}\cdot(\hat{\mathbf{h}}\times\hat{\mathbf{r}})](\cos\nu + \frac{e+\cos\nu}{1+e\cos\nu})\right\} \tag{7}$$

where μ is the gravitational parameter of the Earth. This expression makes use of the Lorentz force, $\mathbf{F_L}$, explicitly.

Equations 3, 4, 6, and 7 are greatly simplified if we restrict our discussion to circular (or near circular) orbits, where the term $(\mathbf{r}\cdot\mathbf{v})$ vanishes. Applying this simplification to Eq. 3 yields

$$\dot{E} = \frac{q}{m}\omega_E\sqrt{\frac{\mu}{r^3}}\sin i\cos u(\mathbf{B}\cdot\hat{\mathbf{r}}) \tag{8}$$

where u is the argument of latitude of the spacecraft. The argument of latitude is defined as the angle from the point of right ascension to the spacecraft's position, measured around the orbit. The orbital energy of a circular LAO is affected by only the radial component of the magnetic field. Thus, orbital energy change is greatest near the poles and goes to zero at the magnetic equator. Additionally, if the same simplification is applied to Eq. 4, we find that the change in scalar angular momentum is simply a multiple of the change in energy:

$$\dot{h} = \sqrt{\frac{r^3}{\mu}}\dot{E} \tag{9}$$

The inclination change in a circular orbit follows the same pattern:

$$\frac{di}{dt} = \frac{\frac{\omega_E r^2}{h}\cos i - 1}{h\omega_E\sin i}\dot{E} \tag{10}$$

Equation 10 implies that, in circular orbits, orbital energy and inclination are not independently controllable. For every increase in energy, there is a corresponding decrease in inclination. (This fact also holds true for any polar orbit, eccentric or not.) This correlation limits the maneuvers that can be performed with an LAO.

Change in eccentricity is also examined under the circular-orbit assumption. Simplifying Eq. 7 yields

$$\begin{aligned}\dot{e} &= \frac{q}{m}\frac{h}{\mu}\Bigg\{2\frac{\omega_E}{h}\sqrt{\frac{a}{\mu}}r^2\sin i\cos(\theta-\Omega)\sin\phi\cos\nu(\mathbf{B}\cdot\hat{\mathbf{r}}) \\ &\quad +\sin\nu\left(\omega_E r\sin\phi-\frac{h}{r}\frac{\cos i}{\sin\phi}\right)(\mathbf{B}\cdot\hat{\phi})-\frac{h}{r}\sin i\cos(\theta-\Omega)\sin\nu(\mathbf{B}\cdot\hat{\theta})\Bigg\} \qquad (11)\end{aligned}$$

The change in eccentricity depends on all three components of the magnetic field, making for more complicated analysis. Each term in Eq. 11 involves the true anomaly, ν. This relationship shows the importance of radial velocity, which is also explicitly related to ν. Changes in eccentricity are thus driven by small deviations from the circular-orbit assumption.

The Geomagnetic Field

The simplest frequently used model of the Earth's magnetic field is a dipole aligned with Earth's spin axis. However, this simple model fails to describe several important behaviors in an LAO. The Earth's magnetic field is best described as a spherical harmonic expansion.[11] The full expansion captures two important features: that the dipole component is not aligned with the Earth's spin axis and that terms higher in degree than the dipole are significant components of the field. Here, spherical harmonic coefficients released as the International Geomagnetic Reference Field are used,[12] in particular, the IGRF95 (or IGRF-7) model. All simulations in this study use coefficients up to 10th degree and order. An important note on the magnetic field is that it is represented in Earth-fixed coordinates. The field itself is locked in step with the rotation of the Earth.[13] We must be careful to distinguish between Earth-fixed longitudes and inertial longitudes.

The effect of the Lorentz force on an orbit is naturally broken up into the components of the magnetic field in spherical-coordinate unit vectors: the radial direction $\hat{\mathbf{r}}$, the colatitude direction $\hat{\phi}$, and the azimuthal direction $\hat{\theta}$. The magnetic field, $\mathbf{B}$, is studied as the three components $(\mathbf{B}\cdot\hat{\mathbf{r}})$, $(\mathbf{B}\cdot\hat{\phi})$, and $(\mathbf{B}\cdot\hat{\theta})$. Figure 2 shows a contour plot of $(\mathbf{B}\cdot\hat{\mathbf{r}})$ over (Earth-fixed) latitude and longitude. Positive values are represented by red contours and negative contours are dotted grey. The black contour has value of zero. This contour is referred to as the magnetic equator. On this line the field has no radial component. In traditional terms, the magnetic equator is where the field has no inclination (or "dip"). For an axis-aligned dipole model, the magnetic equator would lie on the true equator, but the additional higher-degree terms modify its location significantly.

Figure 3 shows a contour plot of $(\mathbf{B}\cdot\hat{\phi})$. Again, grey contours are negative and red positive, with black being zero. The $\hat{\phi}$-component of the field is generally negative, except for small polar regions. The $\hat{\phi}$-component is small near these polar regions and is largest near the magnetic equator.

Figure 4 shows a contour plot of $(\mathbf{B}\cdot\hat{\theta})$. The contour colors are as above. Figure 4 shows distinct regions of positive and negative values. The zero contour represents the line of zero declination (or zero difference between true north and magnetic north). The dipole component of the field (and all other zero-order terms) contributes nothing to the $\hat{\theta}$-component of the field.

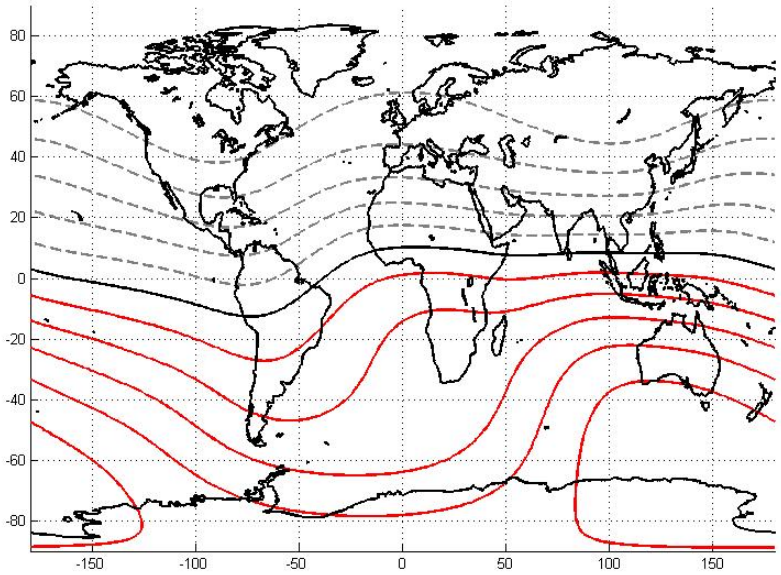

Figure 2 Contour plot of the radial component of the geomagnetic field over latitude and longitude. The black contour represents zero. The dotted grey contours are values less than zero; the red contours are values greater than zero.

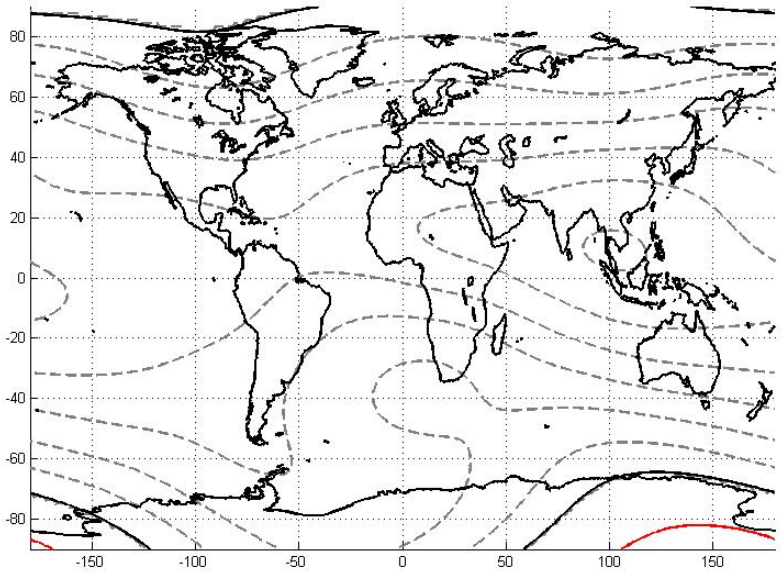

Figure 3 Contour plot of the component of the geomagnetic field in the $\hat{\phi}$ direction over latitude and longitude. The black contour represents zero. The dotted grey contours are values less than zero; the red contours are values greater than zero.

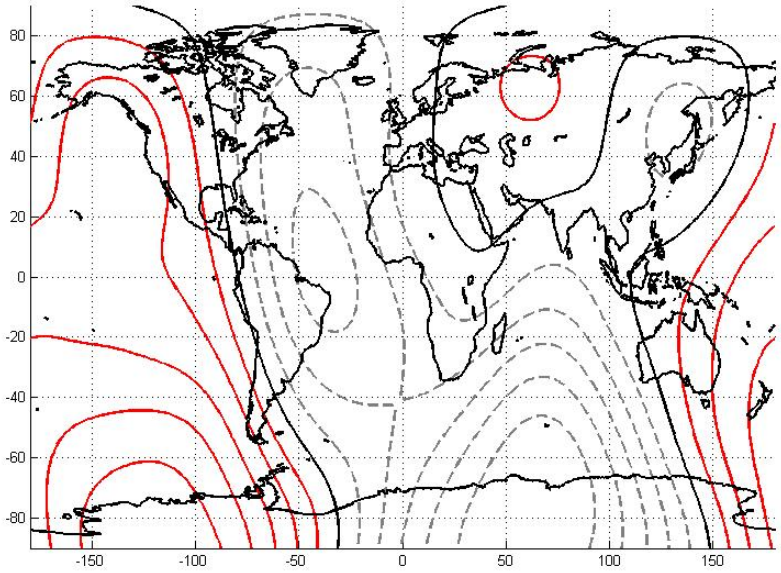

Figure 4 Contour plot of the component of the geomagnetic field in the $\hat{\theta}$ direction over latitude and longitude. The black contour represents zero. The dotted grey contours are values less than zero; the red contours are values greater than zero.

The three orthogonal components of the field can be used to divide the space of latitude and longitude into eight distinct zones. The zones are defined by whether each component is positive or negative and are bounded by the zero contours depicted in Figs. 2, 3, and 4. The zones are numbered I-VIII and depicted graphically in Fig. 5 with properties shown in Table 1. Figure 5 shows each of the zones superimposed on a map of the Earth. Because of distortion do to the map projection, Zones I, II, VII, and VIII are shown larger than their actual sizes. In a 3-dimensional view, they appear in a small region near each pole. The large southward swing of the zero-declination contour over eastern Africa actually crosses the magnetic equator, causing zones III and V to have non-contiguous regions. Table 1 lists the differences between the zones. A '+' in the table refers to a quantity greater than zero, while a '-' denotes less than zero.

Table 1 Zone Properties

Zone	$(\mathbf{B} \cdot \hat{\mathbf{r}})$	$(\mathbf{B} \cdot \hat{\phi})$	$(\mathbf{B} \cdot \hat{\theta})$
I	+	+	+
II	+	+	−
III	+	−	+
IV	+	−	−
V	−	−	−
VI	−	−	+
VII	−	+	−
VIII	−	+	+

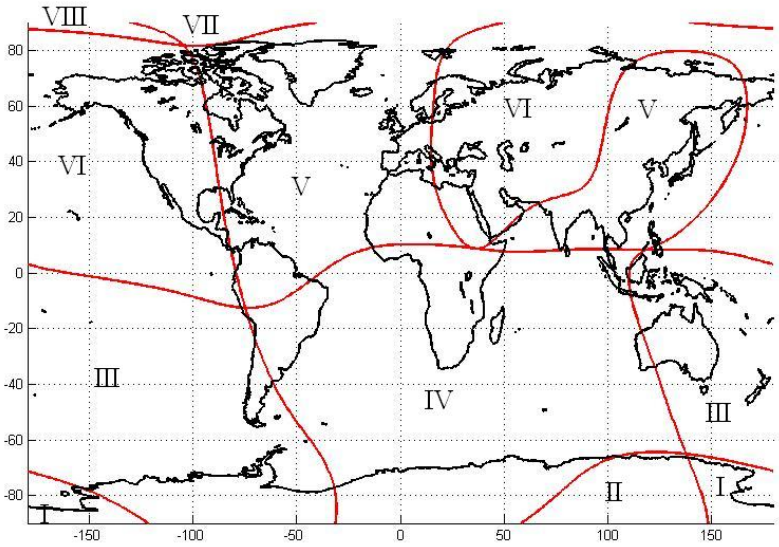

Figure 5 Eight distinct zones of the geomagnetic field, numbered I-VIII. The zone properties are enumerated in Table 1

In each Zone I-VIII, the geomagnetic field has a certain sign for a particular component of the field. Each zone creates different effects on the orbit of a charged satellite. We use these differences to create a control sequence to perform a desired maneuver. The zones are defined with respect Earth-fixed latitude and longitude as the geomagnetic field rotates with the Earth. The contour plots above are for a representative altitude (400 km) because the relative strength of each order of field terms depends on this altitude. However, the zones at any particular location are easily calculated by the simple sign definitions shown in Table 1.

SPACE VEHICLE DESIGN

This section offers a brief overview of possible architectures for LAO capable spacecraft. It considers three competing, interrelated parameters: capacitance, power, and space-vehicle mass. There are also issues of implementation, such as deployability of the capacitor, technology readiness of the power system, thermal implications of high power, and interactions among various subsystems (notably attitude control). We intend to discuss these implementation issues in depth in a future work. For the present, maximizing the $\frac{q}{m}$ metric is taken to be the only goal of LAO space vehicle design. Furthermore, we consider this metric only in terms of a constant-mass spacecraft. 500 kg is chosen as a somewhat arbitrary constraint for this mass optimization. The mass is given some contingency. We consider two degrees of conservatism in this contingency, as explained below.

Capacitance

High $\frac{q}{m}$ implies high charge, which requires high capacitance. Known technologies for self-capacitance store charge on the surface of a conductor with no sharp local features or high curvature. So, one seeks high surface area to volume in flat structures or long, thin ones. Such a capacitor

likely encounters a limit associated with the minimum thickness of thin films or the minimum feasible diameter of long filaments. That limit ultimately leads to a minimum mass for the capacitor. The capacitor is also designed to exploit plasma interactions. Inspired by results from the University of Michigan,[14] we have baselined a cylindrical capacitor constructed of a sparse wire mesh. This stocking-like arrangement of appropriately spaced thin wires develops a plasma sheath due to ionospheric interactions that raises the capacitance of the cylinder well above what it would be in a pure vacuum.

In this model, the capacitance C is taken to be that of a solid cylinder of the stocking's radius R but with a concentric shell (due to the plasma sheath) equal to the thickness of an individual wire's sheath r_s:

$$C = \frac{2\pi\epsilon_0 L}{\log \frac{R+r_s}{R}} \tag{12}$$

where ϵ_0 is the permittivity of free space. The sheath radius increases with potential and is calculated as described by Choiniere.[14] We space these wires so that one wire is a sheath's thickness away from its neighbor. This spacing ensures overlap between individual wires' sheaths but keeps the structure sparse. Occasional structural elements, such as thin conductive bands, would be necessary to maintain the spacing along the capacitor because of Coulomb repulsion that acts among the wires. This repulsion would also serve as a useful means for deploying the capacitor without heavy trusses or actuators.

Power

We consider two fundamentally different approaches to the power subsystem. The classical approach depends on solar power. Energy from solar panels is used directly to power the capacitor, countering the plasma currents, or is stored in batteries or some sort of efficient ultracapacitor to be used in a periodic-charging scheme. Some assumptions about the specific power (W/kg) must be made. We consider a near-term power density of 40 W/kg[15] and a farther-term power density of 130 W/kg, consistent with DARPA's FAST program.[16]

In the case of this classical approach, the charge is maintained by modifying the current collection scheme proposed by Sanmartin, et al.[17] A power supply on board the spacecraft establishes a potential between two conductive surfaces exposed to the plasma environment. The positive end attracts the highly mobile electrons, while the negative end attracts the far less mobile ions (such as O^+). The substantial imbalance in electron and ion currents leads the negative end to accumulate a nonzero charge while the positive end is almost electrically grounded in the plasma. So, with the wire capacitor on the negative end, the spacecraft would achieve a net charge roughly equal to the product of the capacitance of the wires and the potential across the power supply. This charge is accomplished without the use of particle beams.

A more unusual approach exploits alpha-particle emission from an appropriate radioactive isotope,[18] such as Po 210. These emissions are not converted to electrical power thermionically as in a radioisotope thermoelectric generator (RTG) or via fission in a nuclear reactor; instead, the isotope is spread thinly enough on the capacitor's surface that up to half of the emitted alpha particles carry charge away from the spacecraft. The electrical current of these particles is proportional to their charge (2 positive fundamental charges), their kinetic energy (roughly 5.3×10^6 eV), and the isotope's decay rate. If the maximum potential can be achieved despite currents from the surrounding ionospheric plasma, this approach offers as much as 42 kW/kg of Po 210 after 1 year of alpha

decay. Maintaining this charge requires no power supply. The spatially distributed nature of the current from the thin film suggests that the current does not approach any sort of beam-density limit due to space charge.

We focus on the prospects for the classical approach because launching an isotope is likely to encounter a variety of technical and non-technical roadblocks. Both approaches are required to combat the incoming ion currents from the plasma. In all cases, the capacitor exhibits negative charge. The ion currents are then given by the Orbit Motion Limited (OML) estimate.[14] We use the International Reference Ionosphere (IRI)[19] to provide the necessary plasma number density and temperature. We also account for the photoelectron current emitted from the surface of the conductive capacitor. In the case of the classical approach, all of this power is subject to resistive losses as the power supply drives current through the many, thin wires. Assuming that the current is uniform to all parts of the capacitor, we average the losses along the length of wire that the current has to travel.

Space Vehicle Mass

The charge-to-mass ratio depends on the mass of the entire space vehicle. We model this mass coarsely, as the sum of discrete components with interrelated dependencies. Table 2 summarizes this mass model.

Table 2 Space Vehicle Mass Model

Subsystem or Component	Conservatism		Units
	High	Low	
Payload	50	50	kg
Bus (w/ payload power)	3.33	3.33	(kg bus) /(kg payload)
LAO Solar Power	0.025	0.0077	kg/W of orbit-average power
LAO Isotope Power	42	42	kW/kg of Polonium after 1 year of decay
Power Mass Contingency	0.1	0.1	(kg contingency) / (kg LAO power mass)
Capacitor	$2700\pi R^2 nL$	$2700\pi R^2 nL$	kg for n aluminum wires of length L and radius R
Capacitor Mass Contingency	$3m + 50$	$1.1m$	kg, where m is the sum of the wires' masses

An example of the power calculation for the minimally conservative calculations is shown in Table 3. Table 4 uses this power calculation to arrive at the 500 kg space-vehicle mass requirement.

Performance Estimates

These figures summarize the results of these calculations for a 500 kg spacecraft that charges for 20% (uniformly distributed) over a 600 km orbit. Figure 6 shows the low-conservatism design, which yields $\frac{q}{m} = 0.01$ C/kg for a 21 km stocking at 7 kV potential. That level of charge requires an orbit average power of 29 kW. Figure 7 shows the high-conservatism design. For that case,

Table 3 Example of Power Calculation for Low Conservatism

Parameter	**Value**	**Units**
Wire Material	Aluminum	
Wire Radius	5.00×10^{-6}	m
% Overlap Sheath Diameter	0%	
Low-Conservatism Stocking Mass Contingency	118.79	kg
Length of Stocking	21338	m
Cage Radius as a % of Stocking Length	5.00%	
Low Conservatism Stocking Mass Sandbag	3.44	kg
% of Full Ion Current Collection	100%	
Intermediate Calculation	**Value**	**Units**
Material Resistivity at 20°C	2.82×10^{-8}	Ω
Radius of Stocking	1067	m
Material Density of Wire	2700	kg/m^3
Sheath Thickness	1.764	m
Resistance per Wire	7.661	MΩ
Number of Wires	7601	
Mass of Stocking	34.39	kg
Mass of Capacitor	37.83	kg
Cylinder-as-body Capacitance	7.18×10^{-4}	F
Result	**Value**	**Units**
Body Charge	5.028	C
Plasma Ion Current with N_e Limit	11.257	A
Exposed Wire Area	2548	m^2
Photoelectron Current	0.122	A
I^{2}R Power Loss	65.263	kW
Power Required while Charged	144.92	kW
Orbit-Average Power (20% duty cycle)	**28.894**	**kW**

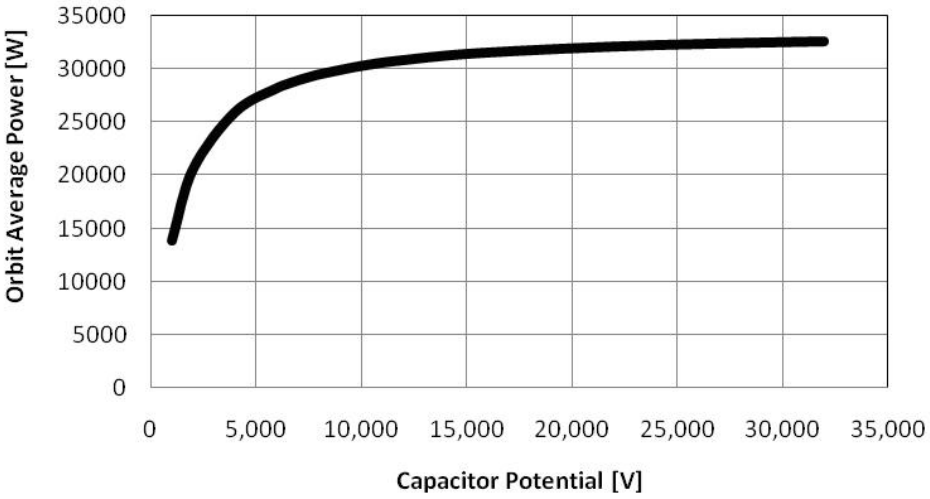

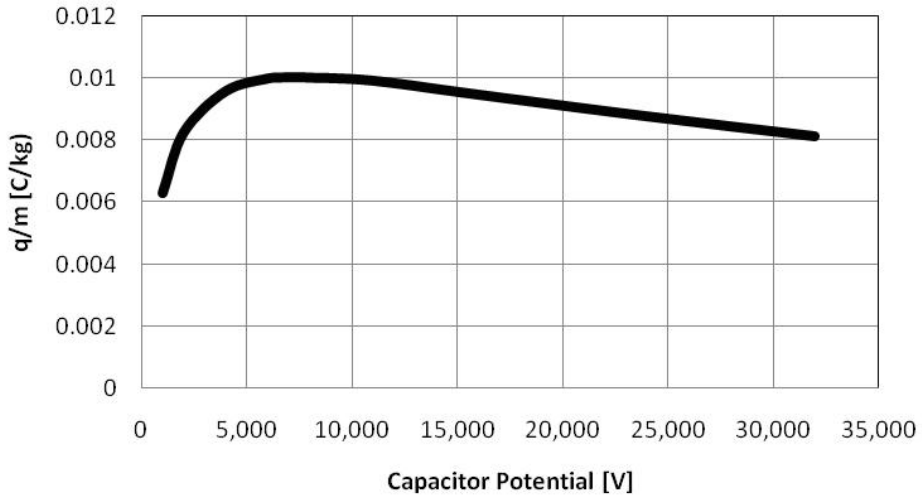

Figure 6 Low-Conservatism Design: Orbit Average Power and $\frac{q}{m}$ vs. Capacitor Potential; Optimum is 0.01 C/kg at 7 kV, which requires 29 kW.

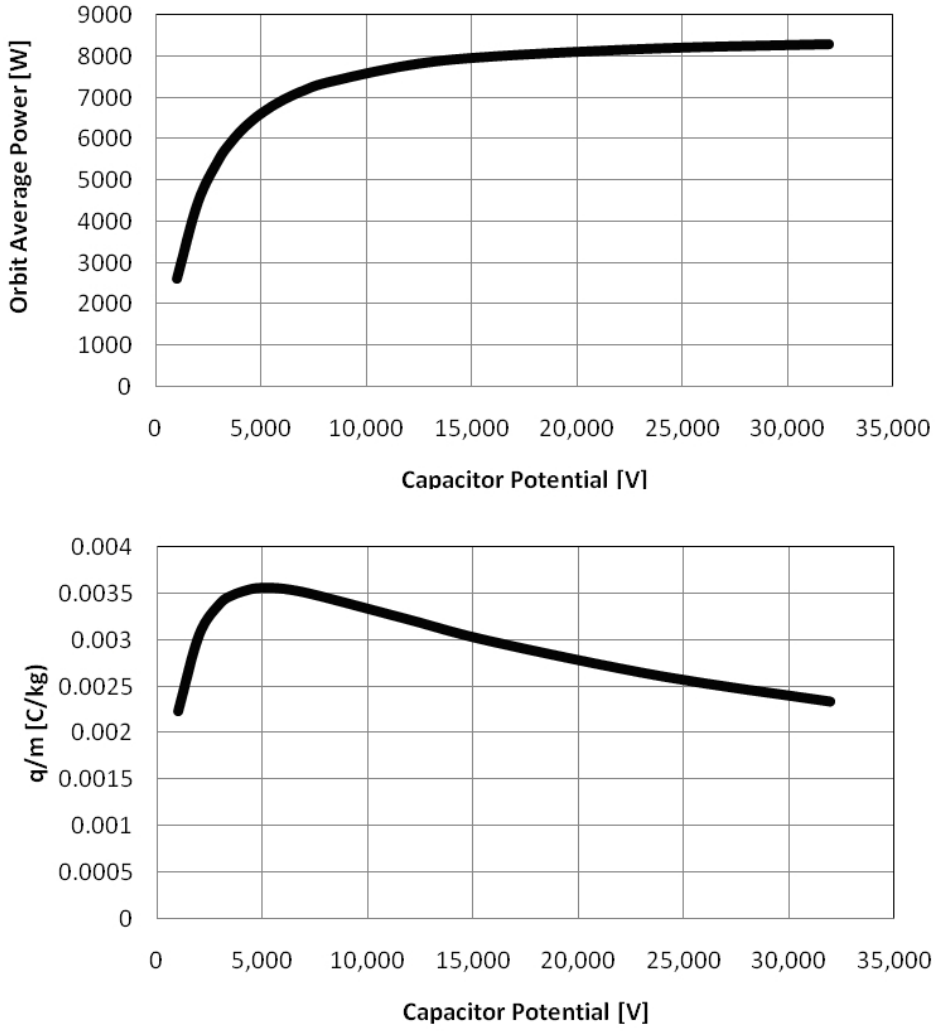

Figure 7 High-Conservatism Design: Orbit Average Power and $\frac{q}{m}$ vs. Capacitor Potential; Optimum is 0.0036 C/kg at 5 kV, which requires 6.6 kW.

Table 4 Example of Mass Calculation for Low Conservatism

Parameter	Value	Units
Potential	-7000	V
Orbit-Average Power for LAO	28984	W
LAO Power System Mass Dependency	0.0077	kg/W
LAO Power System Mass	223	kg
Power System Mass Contingency	22	kg
Payload	50	kg
Buss Mass (including any propellant)	167	kg
Total Space Vehicle Mass	**500**	**kg**

$\frac{q}{m} = 0.0036$ C/kg with a 13 km stocking at 5 kV, which requires an orbit average power of only 6.6kW. In both cases, the efficiency (force per power) increases with lower potential. For example, in the low-conservatism case, the optimal value of 5 C in a 600 km polar orbit produces about 2.3N, for 1.6×10^{-5} N/W when the capacitor is charged. However, at only 1 kV, the resulting 3.1 C represents 2×10^{-5} N/W. So, if the speed of the maneuver is unimportant, lower-potential designs may be better. As the capacitor potential increases beyond the optimum for $\frac{q}{m}$, more mass of the fixed 500 kg must be devoted to the power subsystem, which comes at the expense of capacitor mass.

LAO APPLICATIONS

Maneuver Limitations

Lorentz augmented orbits cannot produce arbitrary changes in an orbit for all given initial conditions. In certain regimes, as evidenced by Eq. 10, changes in orbital elements are tightly coupled. This coupling stems from the basic physics of the Lorentz force. The direction of the force is set by the magnetic field and the velocity of the spacecraft with respect to that magnetic field, neither of which can be altered by the spacecraft control system.

A further limiting factor is that the best system architectures provide only one polarity of charge (negative). Due to the nature of the plasma around the Earth, significantly less power is required to maintain a negative charge than a positive charge. The single-polarity system limits what changes can be made to the right ascension of the ascending node, Ω, and the argument of perigee, ω. For a given charge polarity, Ω and ω evolves only in a single direction. For a negative charge, Ω always decreases and ω always increases.

Table 5 summarizes some of the abilities and limits of LAO for a single polarity of charge. The first column of the table shows the net effect of having a constant charge on a spacecraft. The second column shows the available directions of change for each orbital element for a variable (but single-polarity) charge. The final column summarizes some the special cases and coupling within the dynamics. Some of these special cases are addressed more explicitly in our earlier work.[2,3]

Example Maneuver: LEO Inclination Change

The minimum inclination a spacecraft can be launched into is equal to the latitude of its launch site. For a United States launch, this minimum inclination is generally $28.5°$, the latitude of Cape

Table 5 LAO Effects for $\frac{q}{m} < 0$

Element	Net Effect of Constant Charge	Signs of Possible Changes	Notes
a	0	$+/-$	a/i coupled for $e = 0$ or $i = 90°$, $\dot{a} = 0$ for $i = 0°$ and $e = 0$
e	0	$+/-$	$\dot{e} > 0$ for $e = 0$
i	0	$+/-$	a/i coupled for $e = 0$ or $i = 90°$
Ω	$-$	$-$	Ω undefined for $i = 0°$
ω	$+$	$+$	ω undefined for $i = 0°$ and $e = 0$
ν	0	$+/-$	

Canaveral, FL. However, for certain missions, equatorial orbits are desirable. The plane change between $i = 28.5°$ and $i = 0°$ is expensive in terms of ΔV and requires either a launch vehicle upper stage or a significant expenditure of spacecraft resources. We develop a control algorithm to use the Lorentz force to perform this inclination change without the use of propellant.

This maneuver is primarily concerned with inclination change in circular orbit. Equation 10 describes the relevant dynamics. As energy change and inclination change are coupled in this situation, Eq. 8 describes both the energy and plane changes. In this circular case, only the radial component of the magnetic field affects the energy and inclination. For the inclination to decrease, the energy must increase. Using $\frac{q}{m} < 0$, the term $\cos u(\mathbf{B} \cdot \hat{\mathbf{r}})$ must be negative. We know that $(\mathbf{B} \cdot \hat{\mathbf{r}})$ is positive below the magnetic equator (Zones I, II, III, and IV) and negative above the magnetic equator (Zones V, VI, VII, and VIII). Thus, for northward motion of the satellite ($\cos u > 0$), the charge should be nonzero within Zones V-VIII. For southward satellite motion ($\cos u < 0$), nonzero charge is applied in Zones I-IV. In other words, the charge should be off for the first quadrant of the orbit, on for the second quadrant, off for the third, and on for the fourth.

However, when this simple quadrant control is used, the eccentricity of the orbit tends to grow undesirably large. Maintaining an identically zero eccentricity is impossible, though. Any charge on a circular-orbiting spacecraft causes an increase in the eccentricity. However, we can bound the eccentricity to a small value. Examining Eq. 11, we find that, as the orbit approaches equatorial, the term involving $(\mathbf{B} \cdot \hat{\phi})$ dominates the eccentricity increase. As $(\mathbf{B} \cdot \hat{\phi})$ is of a single sign for most latitudes (see Fig. 3), the sign of this term corresponds to the sign of $\sin \nu$. In turn, the sign of $\sin \nu$ exactly follows the sign of the radial velocity, $\dot{r}$. For positive radial velocity (away from the center of the Earth) and negative charge, the eccentricity change is negative. For negative radial velocity and negative charge, the eccentricity change is positive. These two facts inspire a control algorithm that limits eccentricity growth. This e-limiting algorithm is superimposed over the quadrant control above. First a maximum desired eccentricity, e_{max}, is defined. When e_{max} is approached, charge is applied only if the radial velocity of the spacecraft is greater than zero, causing the eccentricity to decrease. With e now below e_{max}, the charge can be applied as required by the quadrant method until e_{max} is approached again. This e-limiting quadrant control has performance in changing a and i that is close to the unmodified control.

Figure 8 shows the results of a simulation using the e-limiting quadrant method. The simulation begins with a 600 km altitude circular orbit. The charge-to-mass ratio is $\frac{q}{m} = -0.01$ C/kg. The maximum eccentricity is $e_{max} = 5 \times 10^{-4}$. The simulation lasts for one year. The IGRF95 magnetic

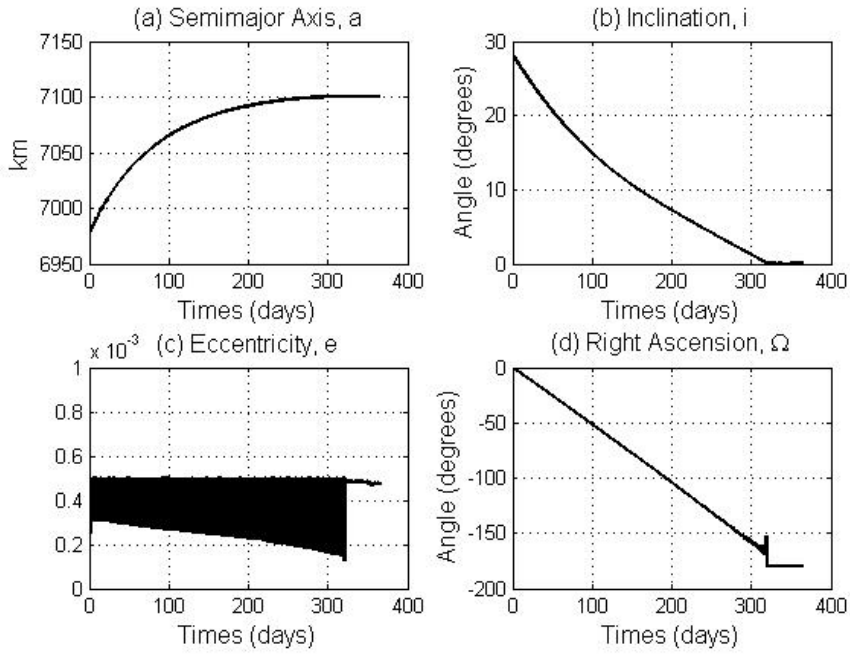

Figure 8 Orbital elements for the LEO plane change maneuver. Plot (a) is the semi-major axis, plot (b) is the inclination, plot (c) is the orbital eccentricity, and plot (d) is the right ascension.

field model is used to 10th degree and order. In Fig. 8, plot (a) shows the increase in semimajor axis given by the quadrant method. The initial 600 km orbit is raised to a 722.4 km circular orbit, in increase of 122.4 km. Plot (b) shows the desired decrease in inclination angle. Since the magnetic equator does not align with the true equator, the inclination can be brought down to exactly zero. Zero inclination is reached in about 320 days with this charge. After this milestone is reached, the charge is not turned on again. Figure 8, plot (c), shows the eccentricity. The eccentricity initially grows until it reaches e_{max}, at which point the e-limiting conditions are used. The e-limiting control keeps the eccentricity equal to or below e_{max} for the entirety of the simulation. Finally, Fig. 8, plot (d), shows the right ascension of the orbit. For a negative $\frac{q}{m}$, the right ascension always decreases. Near an equatorial orbit, the right ascension becomes poorly defined.

If the maneuver simulated above is performed using conventional impulsive thrust, it requires a ΔV of 3.75 km/s. Thus using LAO could significantly increase the payload ratio of a spacecraft that needed such a maneuver. However, this mass savings comes at a cost of time spent, the mass of the capacitor, and electrical power consumed during the maneuver.

Example Maneuver: GEO Transfer Inclination Change

Another commonly performed, expensive maneuver is the combined planed change/circularization of a geostationary transfer orbit (GTO) to a geosynchronous orbit. Again, a GEO satellite can be launched only into an orbit with inclination greater than or equal to the latitude of its launch site. The subsequent plane change is expensive to perform. We attempt to perform this inclination change using LAO.

In the LEO plane change maneuver discussed above, inclination change was maximized according to the constraint of keeping the eccentricity below e_{max}. In the GTO maneuver, the initial orbit is highly eccentric. So, no restriction is placed upon eccentricity change. A simple control is used: charge is on whenever Eq. 6 is less than zero (to decrease inclination) and off otherwise.

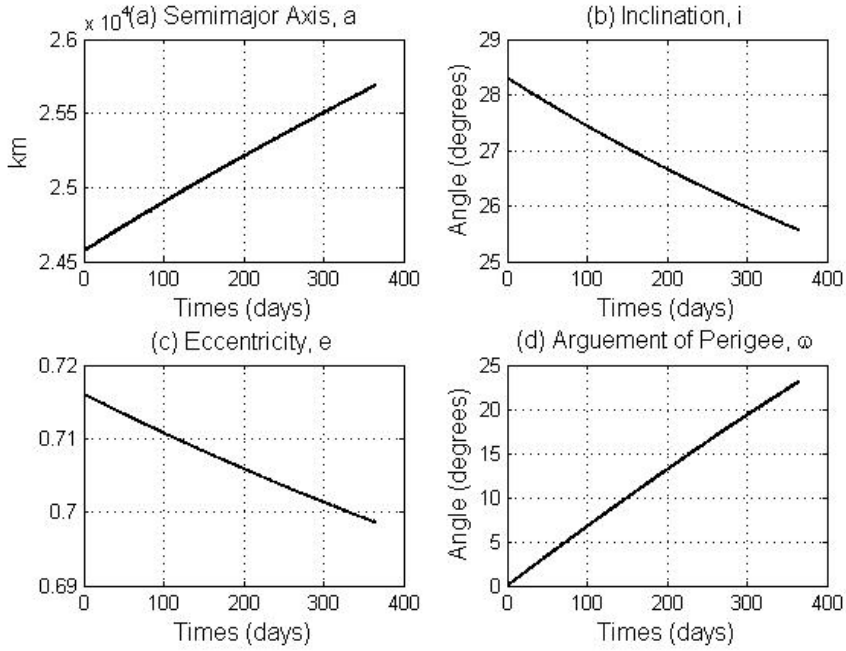

Figure 9 Orbital elements for the GTO plane change maneuver. Plot (a) is the semimajor axis, plot (b) is the inclination, plot (c) is the orbital eccentricity, and plot (d) is the argument of perigee.

The results of a one-year simulation using this controller are shown in Fig. 9. This simulation begins with a GTO orbit (apogee at GEO, perigee at 600 km altitude). The initial inclination is $28.5°$. The charge-to-mass ratio is -0.01 C/kg. In Fig. 9, plot (a) shows the increase in semimajor axis that results from the coupling of inclination and energy changes. The semimajor axis grows by about 1100 km. In the inclined GTO case, the energy change and inclination change are not exactly coupled as in the circular case, but they generally trend inversely. Plot (b) of Fig. 9 displays the desired inclination decrease. However, because the spacecraft spends much of its orbit far from the Earth, the change in inclination is much smaller than over the same time period in LEO. Over the course of one year, the inclination decreases only by $2.74°$. Plot (c) shows the orbital eccentricity over the course of the maneuver. In this case, the eccentricity tends to get smaller, decreasing by 0.017 over the year. Figure 9, plot (d), shows the argument of perigee of the satellite. As the charge is of only one polarity, ω tends to go in only one direction (positively). The change in ω causes the orbit to rotate within the orbital plane.

The GTO inclination maneuver is not as effective as the LEO plane change. By virtue of always remaining at low altitude where the Lorentz force is strongest, the LEO plane change happens 10 times faster. The long time scale of the GTO maneuver makes it impractical to use. After one year, the LAO saves little in terms of propellant used. For the most favorable geometries, the ΔV savings afforded by the LAO maneuver over a conventional propulsive maneuver is only 125.5 m/s.

CONCLUSION

Lorentz Augmented Orbits (LAO) use the Earth's magnetic field to provide propellantless propulsion. While the direction of the Lorentz force is fixed by the velocity of the spacecraft and the local field, varying the magnitude of the charge-to-mass ratio of the satellite can produce novel and useful changes to an orbit. A simple on-off (or bang-bang) charging scheme is sufficient to perform most available maneuvers and can create large savings of ΔV.

A preliminary evaluation of some possible architectures leads us to the tentative conclusion that up to 0.01 C/kg can be reached by a negatively charged LEO spacecraft of 500 kg mass. These designs use cylindrical mesh "stocking" capacitive structures that are shorter than most proposed electrodynamic tethers and offer the important benefit that their performance is independent of their attitude in the magnetic field. That simplicity largely decouples attitude control from propulsion, a consideration that can complicate the operation of tether-driven spacecraft.

The Earth's magnetic field is complex. Accurate analytical expressions for orbital perturbations are difficult to obtain. The geomagnetic field is best examined by breaking it into distinct zones based on its sign in three orthogonal directions, leading to eight zones. Within each zone an LAO tends to evolve in certain directions for certain orbital elements. Understanding how the orbital evolution relates to the zone the spacecraft is in allows us to develop control strategies to execute complex maneuvers. A simple, but effective strategy is to operate a bang-bang control scheme that switches only at zone boundaries. This scheme allows for the execution of a sample maneuver of a LEO plane change without the use of propellant, saving a ΔV of 3.75 km/s required for a conventional propulsive maneuver.

REFERENCES

[1] M. A. Peck, "Prospects and Challenges for Lorentz-Augmented Orbits," *Proceedings of the AIAA Guidance, Navigation, and Control Conference*, San Francisco, CA, AIAA-2005-5995, August 2005.

[2] B. Streetman and M. A. Peck, "New Synchronous Orbits Using the Geomagnetic Lorentz Force," *Journal of Guidance, Control, and Dynamics*, Vol. 30, No. 6, 2007, pp. 1677–1690. AIAA-0731-5090.

[3] B. Streetman and M. A. Peck, "Gravity-Assist Maneuvers Augmented by the Lorentz Force," *Proceedings of the AIAA Guidance, Navigation, and Control Conference*, Hilton Head, SC, AIAA-2007-6846, August 2007.

[4] L. Schaffer and J. A. Burns, "The Dynamics of Weakly Charged Dust: Motion Through Jupiter's Gravitational and Magnetic Fields," *Journal of Geophysical Research*, Vol. 92, 1987, pp. 2264–2280.

[5] L. Schaffer and J. A. Burns, "Charged Dust in Planetary Magnetospheres: Hamiltonian Dynamics and Numerical Simulations for Highly Charged Grains," *Journal of Geophysical Research*, Vol. 99, 1994, pp. 17211–17223.

[6] D. P. Hamilton, "Motion of Dusit in a Planetary Magnetosphere: Orbit-Averaged Equations for Oblateness, Electromagnetic, and Radiation Forces with Applications to Saturn's F Ring," *Icarus*, Vol. 101, 1993, pp. 244–264. Erratum: Icarus 103, pp. 161.

[7] M. L. Cosmo and E. C. Lorenzini, *Tethers in Space Handbook Third Edition*. Huntsville, AL: NASA Marshall Spaceflight Center, 1997. 119-151.

[8] L. B. King, G. G. Parker, S. Deshmukh, and J. Chong, "A Study of Inter-Spacecraft Coulomb Forces and Implications for Formation Flying," *Journal of Propulsion and Power*, Vol. 19, No. 3, 2003, pp. 497–505.

[9] H. Schaub, G. G. Parker, and L. B. King, "Challenges and Prospects of Coulomb Spacecraft Formations," *Proceedings of the AAS John L. Junkins Symposium*, College Station, TX, AAS-03-278, May 2003.

[10] J. A. Burns, "Elementary derivation of the perturbation equations of celestial mechanics," *American Journal of Physics*, Vol. 44, No. 10, 1976, pp. 944–949.

[11] C. M. Roithmayr, "Contributions of Spherical Harmonics to Magnetic and Gravitational Fields," tech. rep., NASA, March 2004. TM-2004-213007.

[12] C. E. Barton, "International Geomagnetic Reference Field : The Seventh Generation," *Journal of Geomagnetism and Geoelectricity*, Vol. 49, No. 2, 1997, pp. 123–148.

[13] P. L. Rothwell, "The superposition of rotating and stationary magnetic sources: Implications for the auroral region," *Physics of Plasmas*, Vol. 10, No. 7, 2003, pp. 2971–2977.

[14] E. Choinière and B. E. Gilchrist, "Self-Consistent 2-D Kinetic Simulations of High-Voltage Plasma Sheaths Surrounding Ion-Attracting Conductive Cylinders in Flowing Plasmas," *IEEE Transactions on Plasma Science*, Vol. 35, No. 1, 2007, pp. 7–22.

[15] J. R. Wertz and W. J. Larson, *Space Mission Analysis and Design*. El Segundo: Microcosm Press, 1999. 141–156.
[16] DARPA Broad Agency Announcement, *Fast Access Spacecraft Testbed (FAST)*, November 2007. BAA 07-65.
[17] J. R. Sanmartin, M. Martinez-Sanchez, and E. Ahedo, "Bare wire anodes for electrodynamic tethers," *Journal of Propulsion Power*, Vol. 9, June 1993, pp. 353–360.
[18] E. G. Linder and S. M. Christian, "The Use of Radioactive Material for the Generation of High Voltage," *Journal of Applied Physics*, Vol. 23, No. 11, 1952, pp. 1213–1216.
[19] D. Bilitza, "International Reference Ionosphere 2000," *Radio Science*, Vol. 36, No. 2, 2001, pp. 261–275.